



Na⁺/K⁺-ATPase α isoform deficiency results in distinct spreading depolarization phenotypes

Clemens Reiffurth^{1,2}, Mesbah Alam³, Mahdi Zahedi-Khorasani⁴, Sebastian Major^{1,2,5} and Jens P Dreier^{1,2,5,6,7} 

Abstract

Compromised Na⁺/K⁺-ATPase function is associated with the occurrence of spreading depolarization (SD). Mutations in ATP1A2, the gene encoding the α 2 isoform of the Na⁺/K⁺-ATPase, were identified in patients with familial hemiplegic migraine type 2 (FHM2), a Mendelian model disease for SD. This suggests a distinct role for the α 2 isoform in modulating SD susceptibility and raises questions about underlying mechanisms including the roles of other Na⁺/K⁺-ATPase α isoforms. Here, we investigated the effects of genetic ablation and pharmacological inhibition of α 1, α 2, and α 3 on SD using heterozygous knock-out mice. We found that only α 2 heterozygous mice displayed higher SD susceptibility when challenged with prolonged extracellular high potassium concentration ([K⁺]_o), a pronounced post SD oligemia and higher SD speed in-vivo. By contrast, under physiological [K⁺]_o, α 2 heterozygous mice showed similar SD susceptibility compared to wild-type littermates. Deficiency of α 3 resulted in increased resistance against electrically induced SD in-vivo, whereas α 1 deficiency did not affect SD. The results support important roles of the α 2 isoform in SD. Moreover, they suggest that specific experimental conditions can be necessary to reveal an inherent SD phenotype by driving a (meta-) stable system into decompensation, reminiscent of the episodic nature of SDs in various diseases.

Keywords

Spreading depolarization, spreading depression, Na,K-ATPase, familial hemiplegic migraine, knock-out mouse model

Received 5 September 2018; Revised 24 January 2019; Accepted 24 January 2019

Introduction

Spreading depolarization (SD) is the generic term for all waves of abrupt, near-complete breakdown of the neuronal transmembrane ion gradients that cause neuronal edema and propagate at about 3 mm/min in cerebral gray matter. The SD continuum describes the spectrum from short-lasting SD in metabolically intact tissue to SD of intermediate duration to terminal SD in severely ischemic tissue. Accordingly, SDs occur in human diseases from the harmless migraine aura to stroke to circulatory arrest, which means that there are overlaps but also large variations in mechanistic aspects along the SD continuum.^{1,2}

The Na⁺/K⁺-ATPase generates the steep transmembrane gradients of the two principal ions, Na⁺ and K⁺, and accounts for ~50% of the brain's ATP consumption under resting conditions.^{3,4} Accordingly, pharmacological Na⁺/K⁺-ATPase inhibition, using cardiac

¹Department of Experimental Neurology, Charité-University Medicine Berlin, Berlin, Germany

²Center for Stroke Research, Charité-University Medicine Berlin, Berlin, Germany

³Department of Neurosurgery, Hannover Medical School, Hannover, Germany

⁴Research Center and Department of Physiology, School of Medicine, Semnan University of Medical Sciences, Semnan, Iran

⁵Department of Neurology, Charité-University Medicine Berlin, Berlin, Germany

⁶Bernstein Center for Computational Neuroscience Berlin, Berlin, Germany

⁷Einstein Center for Neurosciences Berlin, Berlin, Germany

Corresponding author:

Jens P Dreier, Center for Stroke Research Berlin, Department of Neurology, Department of Experimental Neurology, Charitéplatz 1, Berlin 10117, Germany.
Email: jens.dreier@charite.de

glycosides such as ouabain, is known to trigger SD under normoxic conditions⁵ and SD under anoxia/ischemia is assumed to result from failure of the Na⁺/K⁺-ATPase due to lack of ATP.^{6,7} Three distinct α isoforms of the Na⁺/K⁺-ATPase are expressed in the brain by individual genes in a developmentally regulated and cell-type specific manner: α 1, α 2, and α 3.^{8,9} Na⁺/K⁺-ATPase α isoforms vary in their kinetic properties and in their affinity to Na⁺, K⁺, ATP and ouabain.¹⁰ The α 1 isoform can be found on most cell types and is considered to be the housekeeping enzyme. In the adult brain, the α 2 isoform is expressed predominantly on astrocytes, whereas the α 3 isoform is expressed exclusively on neurons.^{8,11} Experimental data suggest that the α 2 isoform exerts specific functions through coupling to secondary active transporters and functional interaction in spatially restricted microdomains^{12–15} and has been reported to co-localize with glutamate reuptake transporters.^{16,17} Association of mutations in the α 2 and α 3 isoform with neurological disorders suggests isoform-specific functions. Whereas mutations in the gene encoding the α 2 isoform have been identified in patients with FHM2, a severe Mendelian form of migraine with aura,¹⁸ mutations in ATP1A3, the gene coding for the α 3 subunit, are linked to rapid-onset dystonia parkinsonism (RODP),¹⁹ alternating hemiplegia of the childhood (AHC)^{20,21} and cerebellar ataxia, areflexia, pes cavus, optic atrophy, and sensorineural hearing loss (CAPOS) syndrome.²²

Two FHM2 knock-in mouse models (α 2^{+/^{W887R}, α 2^{+/^{G301R}) have been reported to exhibit a high SD susceptibility phenotype^{23,24} and both have been shown to have impaired astrocytic glutamate clearance.^{24,25} However, it is unknown how other Na⁺/K⁺-ATPase α isoforms, in particular the neuronal isoform, modulate the SD process and how their role in SD compares to α 2. A similar affinity of cardiac glycosides to α 2 and α 3 has precluded a pharmacological approach to studying distinct isoforms' function. To investigate the roles of the three Na⁺/K⁺-ATPase α isoforms in SD, we employed mice heterozygous for a null mutation in each of the isoform genes.^{14,26} Because all three Na⁺/K⁺-ATPase α isoforms are essential, homozygosity of the null mutation is embryonically or neonatally lethal. By contrast, heterozygous mice do not have an apparent phenotype and breed normally. In acute brain slices and in-vivo experiments, we investigated the effect of genetic and pharmacological reduction of Na⁺/K⁺-ATPase α isoform activity on SD threshold, propagation and recovery.}}

Materials and methods

Animals

The reporting of animal experiments complies with the ARRIVE Guidelines. All animal experiments were

authorized by the animal welfare authorities in Berlin, Germany: Berlin State Office for Health and Social Affairs (LAGeSo), T0311/11 and G0152-11, and all experimental procedures were conducted in accordance with the Charité Animal Welfare Guidelines.

The effects of genetic reduction of Na⁺/K⁺-ATPase α isoforms on SD were studied in α isoform-deficient knock-out mice ($n=340$) bearing a null mutation in one allele of each of the murine orthologous genes: ATP1A1, ATP1A2, and ATP1A3. All three mouse lines employed in this study were genetically engineered, using techniques of targeted disruption and homologous recombination, at the University of Cincinnati, Ohio, USA.^{14,26} Heterozygous animals did not display an apparent clinical phenotype or histological brain anomalies and were fertile. Na⁺/K⁺-ATPase α isoform-deficient mice were backcrossed to (F>9) and maintained on a C57BL/6J (Jackson Laboratory, Bar Harbor, ME, USA) genetic background. Genotyping was performed by PCR as previously described.^{14,26} Adult male mice, 12–18 weeks of age from each line (α 1, α 2, and α 3 heterozygous and wild-type littermates) were used. Animals were housed in groups (at least two animals per cage) under a 12-h light–dark cycle with food and tap water available ad libitum. Due to the effect of sex hormones on migraine prevalence and SD susceptibility,^{27,28} only male mice were used in this study. To compensate for possible differences in genetic background or environmental factors, heterozygous knock-out mice were only compared to their wild-type littermates (WT).²⁹ For in-vivo experiments, additional confirmatory genotyping was performed.

Na⁺/K⁺-ATPase α isoform-deficient mouse line details

Mice deficient for the α 1 isoform (α 1^{+/^{KOE15}, ATP1A1^{+/^{tm1Ling}) bear a mutation in ATP1A1 that results in removal of exons 15 through 18. Western blot analysis of hippocampal whole tissue extracts revealed a reduction of ~70% of the α 1 isoform with no change in α 2 and α 3 isoform levels.^{14,26} Knock-out mice for α 2 (α 2^{+/^{KOE4}, ATP1A2^{+/^{tm1Ling}) were generated by introducing a deletion in exon 4. Although no transcript was detectable in cardiac homogenates,¹⁴ expression of the protein would result in a truncation of the protein after the first transmembrane domain. Protein expression in hippocampal extracts showed a reduction of α 2 by ~50%, no change in α 1, and α 3 with a ~25% lower expression compared to wild types.²⁶ Mice deficient for the α 3 isoform (α 3^{+/^{KOI4}, ATP1A3^{+/^{tm1Ling}) were generated by introducing a point mutation in intron 4 in ATP1A3, causing aberrant mRNA processing that entails an unstable transcript and loss of expression. Hippocampal protein}}}}}}

expression of $\alpha 3$ was shown to be reduced by $\sim 60\%$, $\alpha 1$ was increased by $\sim 35\%$, and the $\alpha 2$ isoform was unchanged compared to wild types.²⁶

Acute brain slice experiments

Animals ($n = 128$) were deeply anesthetized with isoflurane and decapitated. The brain was quickly removed from the skull and transferred into chilled ($0\text{--}4^\circ\text{C}$) carbogenated (5% CO_2 and 95% O_2) artificial cerebrospinal fluid (ACSF). The ACSF contained (in mmol/L) 129 NaCl, 3 KCl, 1.8 MgSO_4 , 1.6 CaCl_2 , 1.25 NaH_2PO_4 , 21 NaHCO_3 , and 10 glucose (pH 7.4). Depending on the protocol, either coronal or transverse acute brain slices with a thickness of $400\ \mu\text{m}$ were prepared using a vibrating blade microtome (Vibroslice, MA752, Campden Instruments, Loughborough, Leics., England). Brain slices were transferred to an interface-type recording chamber and perfused with prewarmed (36°C) carbogenated ACSF in a humidified atmosphere of 95% $\text{O}_2/5\%$ CO_2 . Before starting the recordings, the tissue was allowed to equilibrate for $\sim 60\ \text{min}$.^{30–32} Viability was assessed by stimulating at the boundary of layer VI to the subjacent white matter using a bipolar platinum stimulation electrode (diameter $25\ \mu\text{m}$, tip separation $100\ \mu\text{m}$, single-pulse duration $100\ \mu\text{s}$, intensity $5\text{--}10\ \text{V}$) and recording field potentials in neocortical layers II/III. In horizontal slices, stimulation of the Schaffer collateral pathway in the hippocampus resulted in a population spike (PS) in stratum pyramidale of the CA1 which was used instead. Slices were accepted if stimulation resulted in a field potential amplitude of at least $1.5\ \text{mV}$. Recorded potential changes were amplified (custom-built ISME amplifier), field potentials were low-pass filtered at $3\ \text{kHz}$ and sampled at $10\ \text{kHz}$, ion-selective potentials were low-pass filtered at $30\ \text{Hz}$ and sampled at $100\ \text{Hz}$, displayed on an oscilloscope, digitized (CED-1401, Spike2 software; Cambridge Electronic Design Limited, Milton, Cambridge, England), and stored for off-line analysis. Electrical stimulation pulses were generated using a programmable pulse generator (Master-8, AMPI Instruments, Jerusalem, Israel) connected to a stimulus-isolator (BSI-1, BAK Electronics, Umatilla, FL, USA).

In-vivo: Urethane/ α -chloralose anesthesia

Heterozygous knock-out mice ($n = 73$) were anesthetized with intraperitoneal injection of urethane ($600\ \text{mg/kg}$) and α -chloralose ($50\ \text{mg/kg}$) in $6\ \text{ml/kg}$ saline. An open cranial window was prepared ($2.5 \times 4.5\ \text{mm}$) using a saline-cooled drill to access the neocortex of the right hemisphere (posterior $3.3\ \text{mm}$ to anterior $1.2\ \text{mm}$ from bregma). The dura was removed and great care was taken to avoid triggering premature

SDs. ACSF was topically applied to the brain containing in mmol/L: $127.5\ \text{NaCl}$, $24.5\ \text{NaHCO}_3$, $6.7\ \text{urea}$, $3.7\ \text{glucose}$, $3\ \text{KCl}$, $1.5\ \text{CaCl}_2$, and $1.2\ \text{MgCl}_2$. The ACSF was equilibrated with a gas mixture containing 6.6% O_2 , 5.9% CO_2 , and 87.5% N_2 . A second small (diameter $\sim 1\ \text{mm}$, posterior $3.6\ \text{mm}$, lateral $2.0\ \text{mm}$ from bregma) burr hole allowed for stimulation of the cortex through the intact dura mater. Regional cerebral blood flow (rCBF) was continuously monitored with one laser-Doppler flow (LDF) probe (Periflux 4001, Perimed, Järfälla, Sweden). The subdural direct current-electrocorticography (DC-ECoG) (bandpass: $0\text{--}45\ \text{Hz}$) was recorded using an Ag/AgCl microelectrode. Changes in the extracellular K^+ concentration ($[\text{K}^+]_o$) and the intracortical DC shift (bandpass $0\text{--}45\ \text{Hz}$) were recorded in a cortical depth of $150\ \mu\text{m}$ using two ISMEs, positioned at the opposing ends of the window. A reference electrode (Ag/AgCl pellet) was placed subcutaneously above the nose. Body temperature was maintained at 37°C using a heating pad (Temperature Control FHC, Bowdoinham, ME, USA). The level of anesthesia was assessed by monitoring breathing rate and testing motor responses to foot-pinching. Electrical stimuli of increasing intensity were applied using a bipolar stimulation electrode (tip diameter: $0.2\ \text{mm}$, tip separation: $0.5\ \text{mm}$, model: NE-200, Rhodes Medical Instruments, Summerland, CA, USA) connected to a battery-driven stimulus isolator (BSI-1, BAK Electronics). The stimulation protocol consisted of biphasic pulses of $100\ \text{ms}$ ($\pm 50\ \text{ms}$) duration with exponentially increasing intensities ($20, 30, 40, 50, 60, 80, 100, 150, 200, 260, 340, 450, 600, 800, 1000\ \mu\text{A}$) at 5-min intervals until SD was triggered.³³ SD threshold was defined as the smallest electrical charge (electric current [A] \times time [s]) necessary to trigger an SD. Analog-to-digital conversion was performed using a Power 1401 (Cambridge Electronic Design). $[\text{K}^+]_o$, voltage and rCBF changes were continuously recorded using a personal computer and Spike2 software (version 6, Cambridge Electronic Design). Animals were killed after the experiment by intravenous administration of KCl solution. SD speed was calculated by dividing the distance between the ISME tips by the latency between SD onset as recorded by the occipital and rostral electrode.

Data analysis, visualization and statistical inference

Unless not stated otherwise, all data are given as mean \pm standard deviation. Boxplots show the median and interquartile range (IQR). The whiskers extend to the most extreme data point that is no more than 1.5 times IQR from the edge of the box. More extreme data points (outliers) are shown as gray plus signs. In addition, the arithmetic mean is included as a red

triangle. For clarity, time-series data or related data points with error bars are given as mean±standard error of the mean (SEM). If desired, standard deviation can be calculated as SEM*sqrt(n) using the sample size given in the text. Assessment of data distribution and statistical testing was performed using the scientific Python stack³⁴ and graphs were prepared using Matplotlib.³⁵

Supplementary materials and methods

Further information on data analysis and statistical inference, K⁺-sensitive microelectrodes, [K⁺]_o threshold for SD induction, stimulus-induced [K⁺]_o increases, KCl microinjection SD threshold, intrinsic optical signal (IOS) recordings, in-vivo experiments under isoflurane anesthesia, and Na⁺/K⁺-ATPase activity assay.

Results

Deficiency of the $\alpha 2$ isoform increases SD susceptibility in acute brain slices when exposed to high [K⁺]_o in the bathing medium

To obtain a measure of SD susceptibility in acute brain slices, we raised [K⁺]_o in a stepwise fashion in 30-min intervals until SD occurred (Figure 1(a) to (c)). In most slices, SDs originated in the neocortex and, in contrast to physiological [K⁺]_o, SDs were not confined to the cortex but frequently invaded the hippocampus in coronal or the striatum in transverse brain slices (Figure 1(a)). In slices from $\alpha 2^{+/KOE4}$ mice, SD was initiated at a significantly lower [K⁺]_o (13.0±1.2 mmol/L, *n*=18) compared to their wild-type littermates (WT) (14.9±1.7 mmol/L, *n*=23; *P*=0.001) (Figure 1(d)). The SD threshold reduction was reflected in a significant shortening of the latency to SD occurrence ($\alpha 2^{+/KOE4}$: 62.1±16.0 min, *n*=18; WT: 79.9±21.6 min, *n*=23; *P*=0.004) (Figure 1(e)). These results indicate that $\alpha 2$ haploinsufficiency results in increased SD susceptibility under elevated baseline [K⁺]_o. In contrast to the threshold effect, peak [K⁺]_o and [K⁺]_o undershoot were not significantly affected by $\alpha 2$ deficiency (Figure 1(f) and (g)).

To compare the magnitude of the observed SD effects of genetic $\alpha 2$ isoform reduction with the effect of pharmacological Na⁺/K⁺-ATPase inhibition, we co-applied 5 μmol/L ouabain with the high [K⁺]_o bathing medium of WT brain slices. In this concentration, ouabain blocks most of the $\alpha 2/3$ portion of the Na⁺/K⁺-ATPase activity.^{5,36} The pharmacological effect on SD latency ($\alpha 2^{+/KOE4}$: -22.2%, ouabain: -22.6%) and SD threshold reduction was of similar magnitude compared to genetic $\alpha 2$ isoform reduction observed in $\alpha 2^{+/KOE4}$ mice ($\alpha 2^{+/KOE4}$: -12.7%, ouabain: -16.4%).

To investigate the contribution of the astrocytic ($\alpha 2$) and the neuronal ($\alpha 3$) isoform to the effect of ouabain inhibition, we added 5 μmol/L ouabain to the high [K⁺]_o ACSF of brain slices from $\alpha 2$ -deficient mice. Although adding ouabain to the bathing medium of $\alpha 2^{+/KOE4}$ brain slices further lowered (4.7%) the threshold [K⁺]_o and further reduced the SD latency by 12.7% in $\alpha 2^{+/KOE4}$ compared to WT, these effects were considerably smaller compared to the effect of ouabain in WT slices and did not reach statistical significance (Figure 1(d) and (e)). These results suggest that the facilitating effect of ouabain on SD is mediated via the astrocytic isoform. If the neuronal isoform would be involved, the ouabain effect would be expected to add significantly to the effect of genetic $\alpha 2$ reduction in $\alpha 2^{+/KOE4}$ mice. Instead, the size of the ouabain effect was reduced in $\alpha 2$ -deficient mice, which is consistent with the reduced ouabain receptor availability. Interestingly, only pharmacological Na⁺/K⁺-ATPase inhibition using 5 μmol/L ouabain significantly prolonged SD duration and reduced DC amplitude, whereas genetic $\alpha 2$ reduction did not have these effects (Figure 1(h) and (i)).

Despite the effect of genetic $\alpha 2$ reduction on SD threshold and latency, SD speed was similar in $\alpha 2^{+/KOE4}$ mice compared to WT ($\alpha 2^{+/KOE4}$: 9.2±2.0 mm/min, *n*=16; WT: 8.8±1.5 mm/min, *n*=21; *P*=0.29) under high [K⁺]_o (Figure 1(j)). Because [K⁺]_o elevation exerts a strong effect on SD speed (high [K⁺]_o: 317% of control in 3 mM [K⁺]_o), a significant speed difference is presumably negated by the lower threshold [K⁺]_o in $\alpha 2^{+/KOE4}$ mice; 5 μM ouabain did not have a facilitating effect on SD speed under high [K⁺]_o either (ouabain: 8.3±1.1, *n*=21; control: 8.8±1.5, *n*=21, *P*=0.34).

Deficiency of other Na⁺/K⁺-ATPase α isoforms does not affect SD susceptibility under elevated baseline [K⁺]_o in brain slices

Next, we sought to determine whether the observed SD threshold [K⁺]_o effect in $\alpha 2^{+/KOE4}$ mice was specific to a genetic reduction of this particular isoform or whether the effect could be mimicked by deficiency of the other Na⁺/K⁺-ATPase isoforms expressed in the brain: $\alpha 1$ and $\alpha 3$. To this end, we tested the high [K⁺]_o protocol with $\alpha 1^{+/KOE15}$ and $\alpha 3^{+/KOE14}$ mice and compared the results to their wild-type littermates (WT).

Whereas lower [K⁺]_o triggered SD in $\alpha 2^{+/KOE4}$ mice, we did not find a significant difference between the threshold [K⁺]_o in $\alpha 3^{+/KOE14}$ (103.7±14.3% of WT, *n*_{het}=13, *n*_{WT}=14; *P*=0.5) or $\alpha 1^{+/KOE15}$ (94.2±9.9% of WT, *n*_{het}=6, *n*_{WT}=8; *P*=0.48) compared to WT (Figure 2(a)). These observations were confirmed by the absence of differences in latency to SD initiation

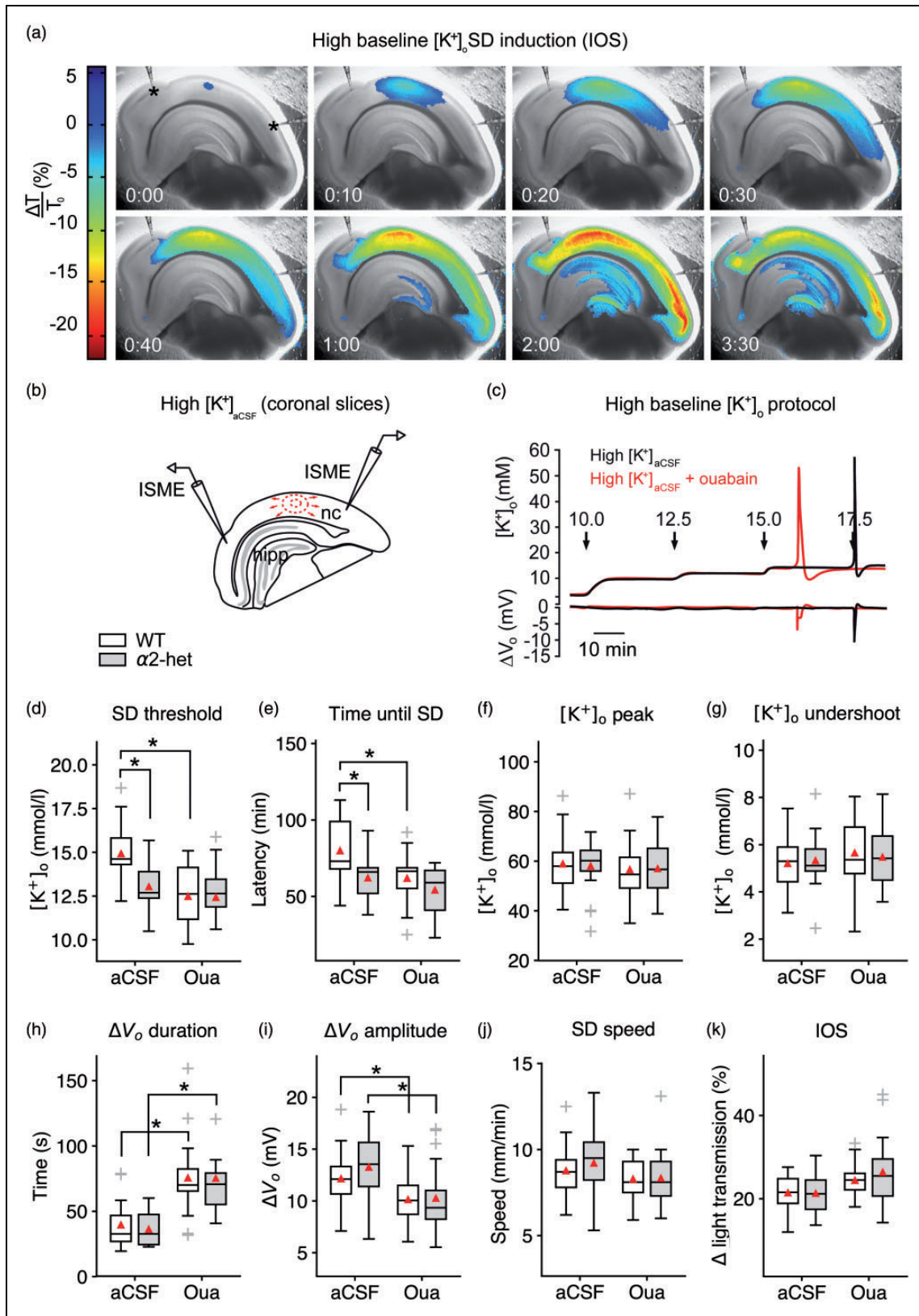


Figure 1. Na^+/K^+ -ATPase $\alpha 2$ deficiency increases SD susceptibility in acute brain slices. (a–b) SD speed and invaded area were imaged using light transmission changes (IOS). In the interface-type recording chamber, SD is characterized by a short increase (blue), followed by a long-lasting decrease of the IOS (red). Elevated baseline $[K^+]_o$ induced SD in the neocortex (nc) and frequently in the

(continued)

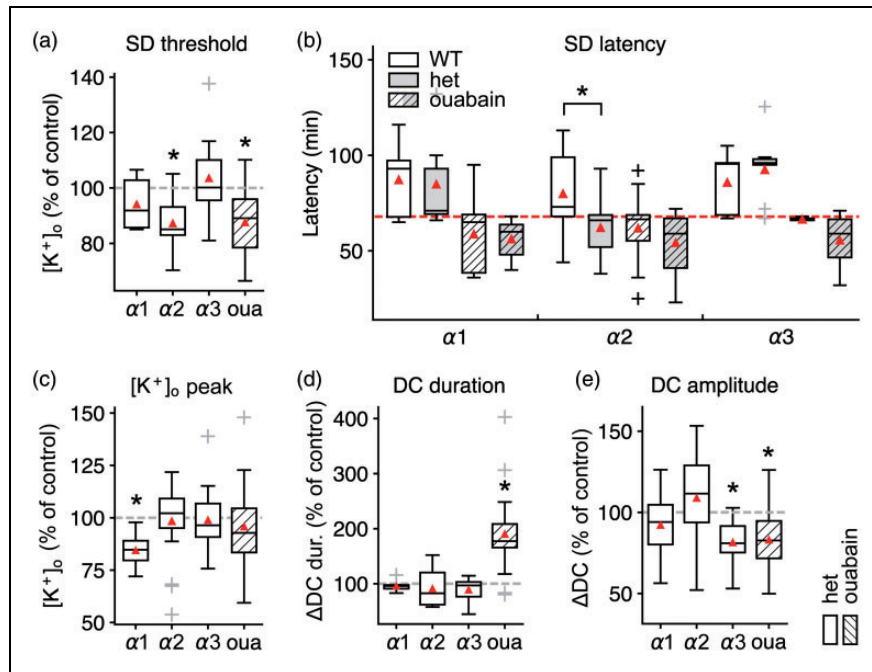


Figure 2. SD threshold reduction is specific to deficiency of the $\alpha 2$ isoform in acute brain slices. (a) Only $\alpha 2$ deficiency or pharmacological inhibition with 5 μM ouabain significantly reduced SD threshold $[\text{K}^+]_o$, whereas $\alpha 1$ and $\alpha 3$ deficiency did not significantly affect threshold $[\text{K}^+]_o$ as measured by ISMEs. (b) SD latency: $\alpha 2^{+/KOE4}$ segregate from the high into the low threshold group together with ouabain, indicated by the significantly shorter time until SD occurrence (below the red dashed line). (c) Peak $[\text{K}^+]_o$ during SD was significantly lower in $\alpha 1^{+/KOE15}$ mice. (d) The duration of the accompanying DC shift was longer only under ouabain exposure, whereas α isoform deficiency had no effect. (e) The DC amplitude was reduced in $\alpha 3^{+/KOE4}$ and in presence of 5 μM ouabain. Sample sizes: $\alpha 2^{+/KOE4}/\alpha 2^{+/+}$, $n = 17\text{--}23$; $\alpha 3^{+/KOE4}/\alpha 3^{+/+}$, $n = 10\text{--}14$; $\alpha 1^{+/KOE15}/\alpha 1^{+/+}$, $n = 6\text{--}8$. * $P < 0.05$.

in $\alpha 3^{+/KOE4}$ and $\alpha 1^{+/KOE15}$ compared to WT (Figure 2(b)). These results indicate that the observed SD facilitation under high $[\text{K}^+]_o$ is specific for a reduction of the $\alpha 2$ isoform and suggest that the effect is not primarily dependent on bulk Na^+ and K^+ transport capacity.

Extracellular K^+ clearance during intense neuronal stimulation is not altered significantly in $\alpha 2^{+/KOE4}$ mice

Because of the effect of $\alpha 2$ deficiency on the SD threshold in conditions of high $[\text{K}^+]_o$ challenge, we wanted to test whether impaired extracellular K^+ clearance was causal to the observed threshold differences. To this end, we analyzed stimulus-induced $[\text{K}^+]_o$ surges during and following intense neuronal stimulation in

acute brain slices (Figure 3(a) to (c)). Stimulus trains of increasing intensity lasting 10 s, consisting of 200 pulses at a frequency of 20 Hz, were applied to the Schaffer collateral pathway in the hippocampal CA1 subfield of transverse brain slices (Figure 3(a)) of $\alpha 2^{+/KOE4}$ and WT. Of note, even under supramaximal stimulation (150%), in none of the $\alpha 2^{+/KOE4}$ slices SD was triggered.

During neuronal activation, K^+ is released into the extracellular space. The $[\text{K}^+]_o$ undershoot following neuronal stimulation is believed to be predominantly attributable to Na^+/K^+ -ATPase activity, stimulated by elevated intracellular sodium concentration ($[\text{Na}^+]_i$) following intense neuronal firing. Because faster K^+ clearance mechanisms, such as passive diffusion and spatial buffering, have redistributed K^+ away

Figure 1. Continued

hippocampus (hipp) but not in the brainstem. (c) Stepwise increased baseline $[\text{K}^+]_o$ allowed for threshold assessment using ISMEs. (d) SD occurred at lower $[\text{K}^+]_{\text{ACSF}}$ in $\alpha 2^{+/KOE4}$ compared to WT. Co-application of 5 μM ouabain did not significantly add to the $\alpha 2$ deficiency effect on threshold $[\text{K}^+]_{\text{ACSF}}$ indicating ouabain action via the astrocytic and not the neuronal isoform. (e) SD latency was shorter in $\alpha 2^{+/KOE4}$ compared to WT mice confirming the lower $[\text{K}^+]_o$ threshold in $\alpha 2$ -deficient mice. (f–g) Genetic $\alpha 2$ reduction did not affect $[\text{K}^+]_o$ peak and $[\text{K}^+]_o$ undershoot following SD. (h–i) Only pharmacological inhibition of the $\alpha 2/3$ portion of the Na^+/K^+ -ATPase prolonged SD duration and decreased the DC amplitude irrespective of the genetic background. (j) SD speed was high under elevated $[\text{K}^+]_{\text{ACSF}}$ without additional effects of genetic or pharmacological $\alpha 2$ reduction. (k) IOS amplitude was not affected significantly by genetic or pharmacological $\alpha 2$ reduction. Sample sizes: $\alpha 2^{+/KOE4}$, $n = 16\text{--}19$; $\alpha 2^{+/+}$, $n = 21\text{--}23$. * $p < 0.05$.

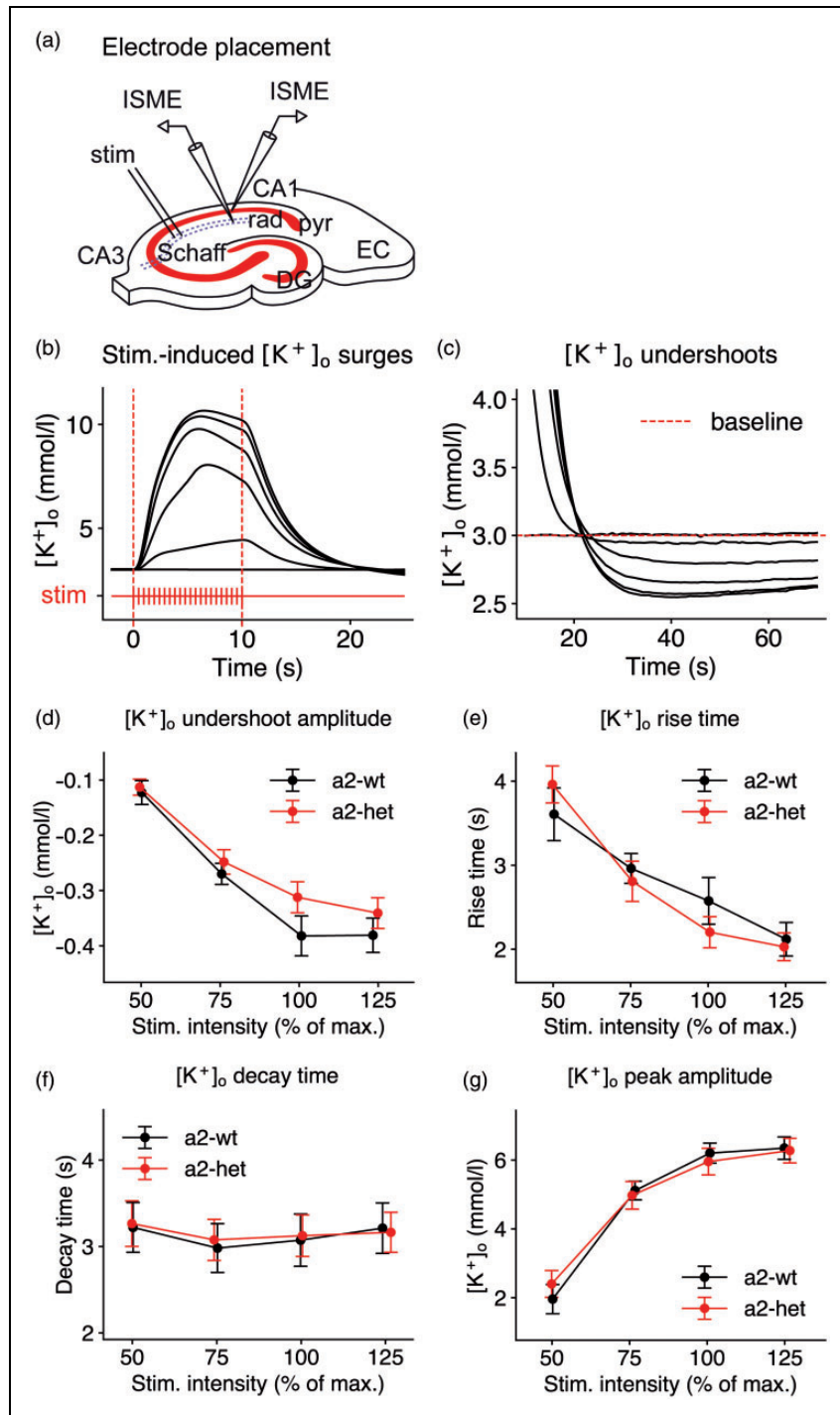


Figure 3. $[K^+]_o$ clearance is not significantly impaired in $\alpha 2$ -deficient mice. (a) A stimulus train (10 s, 20 Hz) was applied to the hippocampal Schaffer collateral pathway (Schaff) in the CA3 of transverse brain slices. stim: bipolar stimulation electrode location; rad: stratum radiatum; pyr: stratum pyramidale; EC: entorhinal cortex; DG: dentate gyrus. (b) $[K^+]_o$ surges and (c) $[K^+]_o$ undershoots were recorded in str. pyramidale and radiatum in CA1 using ISMEs. (d) The $[K^+]_o$ undershoot amplitude showed a tendency to be less pronounced at 100% stimulation intensity although the difference did not reach statistical significance ($\alpha 2^{+/KOE4}$: -0.31 ± 0.03 , $n = 19$; WT: -0.38 ± 0.04 , $n = 13$; $P = 0.13$). (e-g) $\alpha 2$ deficiency did not significantly alter the $[K^+]_o$ response to intense neuronal stimulation. Data are presented as mean \pm SEM.

from the location of its release, $[K^+]_o$ is decreasing from its baseline level and forms a noticeable undershoot.³⁷ The $[K^+]_o$ undershoot amplitude increased with higher stimulation strength and at 100% stimulation intensity, the amplitude appeared to be slightly lower in $\alpha 2^{+/KOE4}$ animals compared to WT, although the difference did not reach statistical significance (Figure 3(d)).

To test whether the $\alpha 2$ isoform is involved in limiting local K^+ accumulation in response to neuronal stimulation, we analyzed $[K^+]_o$ rise time and peak $[K^+]_o$. To assess extracellular K^+ clearance, we analyzed the $[K^+]_o$ decay time.^{25,38} We did not find significant differences in $[K^+]_o$ rise time, decay time, and peak $[K^+]_o$ amplitude between $\alpha 2^{+/KOE4}$ and WT (Figure 3(e) to (g)). The lack of an effect in acute brain slices corresponds to similar activity of Na^+/K^+ -ATPase $\alpha 2/3$ fraction measured in brain homogenates of $\alpha 2$ and WT (Supplementary Figure 1 and Table 1).

The data indicate that the extracellular K^+ clearance during intense neuronal stimulation is not significantly compromised in $\alpha 2^{+/KOE4}$ mice in normal ACSF. This observation is in agreement with data from $\alpha 2^{+/G301R}$ mice in a similar protocol³⁹ but contrasts with the findings in slices of $\alpha 2^{+/W887R}$ mice, that displayed a higher time constant of the $[K^+]_o$ decay following the stimulation train compared to WT.²⁵

In contrast to high $[K^+]_o$, SD threshold and speed are not affected in $\alpha 2^{+/KOE4}$ mice under physiological $[K^+]_o$

Published FHM mouse models exhibit a high SD susceptibility phenotype characterized by a low SD threshold and increased SD speed^{25,33,40} as well facilitated corticostriatal SD propagation.²⁷

To assess the SD threshold without globally affecting $[K^+]_o$, we injected increasing amounts of KCl (1M) focally into the cortical tissue until SD was triggered under normal $[K^+]_o$ (3 mM) (Figure 4(a) and (b)). In contrast to the higher SD susceptibility under elevated baseline $[K^+]_{ACSF}$, the focal induction duration and thus the injected K^+ volume were similar in $\alpha 2^{+/KOE4}$ mice compared to WT under physiological $[K^+]_o$ (Figure 4(c)). We calculated the SD speed using the SD-associated light transmittance (LT) changes (IOS) in the dorsal and the ventral portion of the propagation path (Figure 4(d)). Although we found significantly higher SD speed in the dorsal compared to ventral portion of the cortex (dorsal: 3.2 ± 0.7 , $n=9$; ventral: 2.4 ± 0.4 , $n=9$; $P=0.01$) (Figure 4(e)), SD speed was not different between $\alpha 2^{+/KOE4}$ and WT ($\alpha 2^{+/KOE4}$: 2.6 ± 0.5 mm/min, $n=9$; WT: 2.8 ± 0.5 mm/min; $P=0.86$) (Figure 4(f)). We also analyzed the extent of SD spread as the projected area of the IOS change on the brain slice surface and did not find an effect of $\alpha 2$

deficiency ($\alpha 2^{+/KOE4}$: 3.3 ± 1.3 mm², $n=10$; WT: 3.9 ± 1.3 mm²; $P=0.38$) (Figure 4(g)). Whereas α isoform deficiency in general did not have an effect on SD speed and extent of SD spread, 5 μ M ouabain increased SD speed significantly and resulted in larger extent of SD spread in brain slices (Figure 4(g) and (h)).

The data indicate that $\alpha 2$ deficiency is well compensated under normal $[K^+]_o$, in contrast to prolonged exposure to elevated baseline $[K^+]_o$. The observation of similar SD susceptibility under normal $[K^+]_o$ is unexpected and differs from studies using brain slices of FHM1⁴⁰ and FHM2²⁵ knock-in mice. Both studies reported a lower SD threshold and higher SD speed albeit using a submerged system and not an interface recording chamber as employed in this study. However, the absence of an effect on SD speed has been reported in another study comparing FHM2 knock-in mice ($\alpha 2^{+/G301R}$) with WT in-vivo,²⁴ indicating possible functional differences between distinct FHM2 missense mutations. Despite the aforementioned differences in the recording chamber setup, we expect the brain slice speed measurement approach to be sensitive enough to detect the reported speed differences, since application of 5 μ M ouabain resulted in a massive speed increase (Figure 4(h)). Furthermore, the measurement uncovered a significant difference between the dorsal and the ventral portion of the mouse cortex which was consistent throughout all mouse lines. Additionally, the dorso-ventral SD speed gradient was also evident as a section-dependence of SD speed in transverse slices (data not shown).

SD susceptibility in-vivo

To test the SD threshold in-vivo, we induced SD electrically in the right hemisphere of urethane/ α -chloralose anesthetized Na^+/K^+ -ATPase α isoform-deficient mice. Biphasic stimuli of increasing strength were applied through a bipolar stimulation electrode until SD was recorded by an intracortical microelectrode in the open cranial window (Figure 5(a)). Because of a possible impact on the SD threshold and a drastically different rCBF response of a secondary SD,⁴¹ we assessed the typical multiphasic rCBF response of the mouse using LDF (Figure 5(b)). To test SD susceptibility under different anesthesia and to precisely check for potential induction of premature SDs during the preparation phase, we induced SDs electrically in animals anesthetized with isoflurane in a second set of experiments. LASCA imaging was employed to map cerebral perfusion levels through the intact skull bone of both hemispheres (Figure 5(c) and (d), Supplementary Figure 2).

Confirming the brain slice experiments in normal ACSF of this study, $\alpha 2$ -deficient mice did not display a reduction in the threshold electric charge to induce

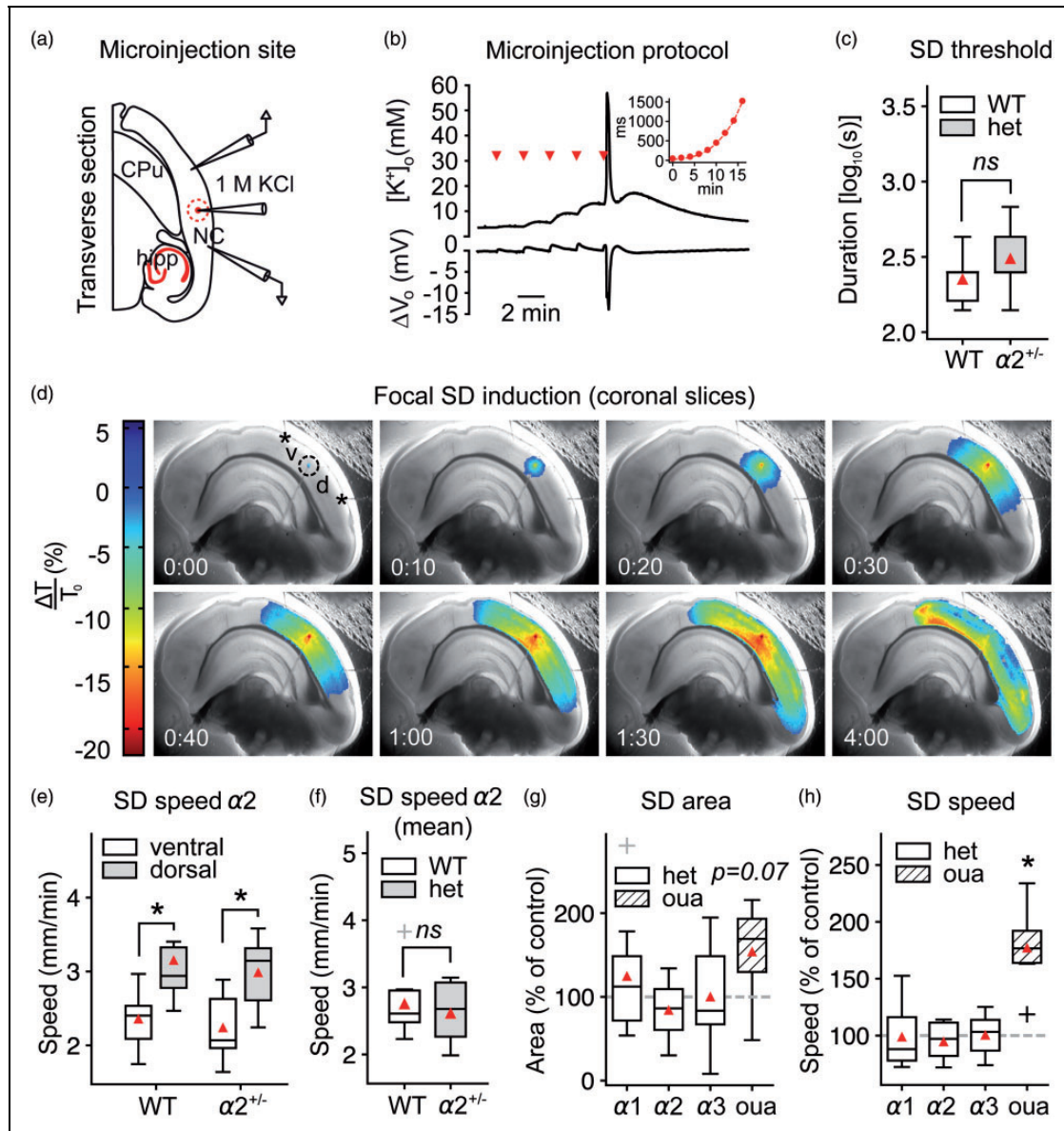


Figure 4. SD speed is not affected by $\alpha 2$ -deficiency in acute brain slices. (a–b) SD was induced focally in acute coronal brain slices under physiological ACSF by microinjecting an increasing volume of 1M KCl into the tissue. NC: neocortex; hipp: hippocampus; CPU: caudate putamen (c) The necessary injected 1M KCl volume to evoke SD was similar in $\alpha 2^{+/KOE4}$ and $\alpha 2^{+/+}$ mice under normal $[K^+]_{ACSF}$ ($\alpha 2^{+/KOE4}$: $n = 9$, $\alpha 2^{+/+}$: $n = 6$). (d) SD speed and area were calculated from the dorsal (“d”) and ventral (“v”) portion relative to injection point (dashed circle) in coronal brain slices. (e) SD propagated with markedly higher speed in the dorsal compared to the ventral portion of the cortex as measured from the injection site. (f) SD speed was not different between $\alpha 2^{+/KOE4}$ and WT (mean of dorsal and ventral speeds) under normal $[K^+]_{ACSF}$. Data were obtained from 9 $\alpha 2^{+/KOE4}$ (39 SDs, 27 slices) and 9 $\alpha 2^{+/+}$ (37 SDs, 25 slices) mice. (g) The projected area of SD spread on the slice surface tended to be larger ($P = 0.07$) only in ouabain-treated slices with no effect in $\alpha 2^{+/KOE4}$ mice. (h) Ouabain application increased SD speed drastically ($77.3 \pm 35.2\%$, $P < 0.00001$), whereas genetic α isoform deficiency had no effect on SD speed. Sample sizes for speed and area calculations: $\alpha 2^{+/KOE4}/\alpha 2^{+/+}$, $n = 9$; $\alpha 3^{+/KOE14}/\alpha 3^{+/+}$, $n = 9$ –16; $\alpha 1^{+/KOE15}/\alpha 1^{+/+}$, $n = 8$; ouabain, $n = 7$. * $P < 0.05$.

SD in-vivo. In fact, the threshold charge tended towards higher threshold charges in $\alpha 2^{+/KOE4}$ mice, although the difference did not reach statistical significance ($\alpha 2^{+/KOE4}$: $58.1 \pm 38.5 \mu C$, $n = 10$, WT: $33.4 \pm 24.3 \mu C$, $n = 12$, $P = 0.15$) (Figure 5(e)). In mice deficient

of the $\alpha 3$ isoform, the SD threshold charge was significantly higher compared to WT ($\alpha 3^{+/KOE14}$: $51.8 \pm 28.3 \mu C$, $n = 9$, WT: $24.0 \pm 14.9 \mu C$, $n = 11$, $P = 0.04$). No effect of α isoform deficiency on SD threshold was observed in $\alpha 1^{+/KOE15}$ compared to WT ($\alpha 1^{+/KOE15}$: $26.5 \pm 16.7 \mu C$,

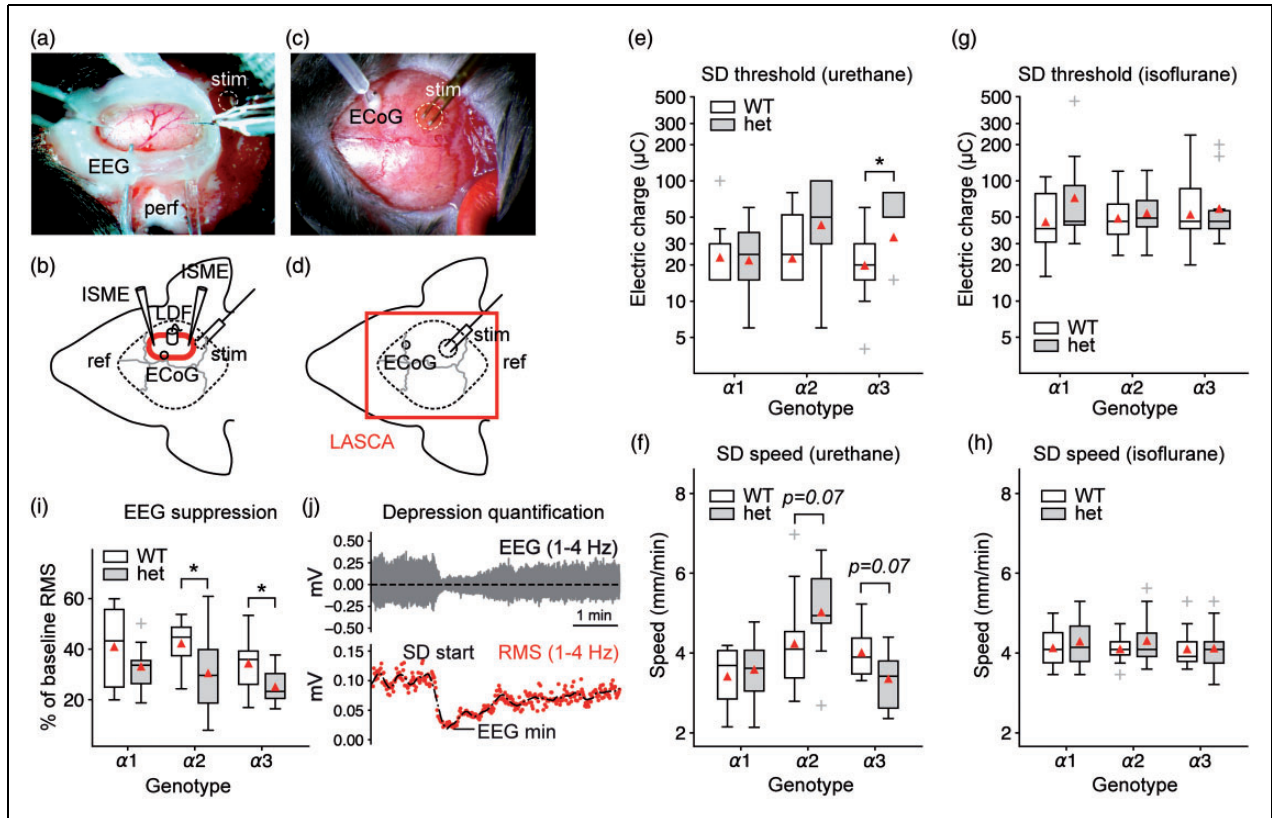


Figure 5. Na^+/K^+ -ATPase α isoform deficiency and anesthesia differentially affect SD threshold and speed. (a–b) Urethane/ α -chloralose protocol with open cranial window preparation and experimental setting. LDF: laser Doppler flowmetry probe; LASCA: laser speckle contrast analysis imaging area; ref: reference electrode; ECoG: electrocorticography electrode; perf: ACSF perfusion; stim: site of electrical stimulation; ECoG: epidurally placed electrode (c–d) Isoflurane protocol with LASCA imaging through the intact mouse skull. (e) In agreement with acute brain slice experiments under normal $[\text{K}^+]_o$, $\alpha 2^{+/KOE4}$ mice do not display a lower SD threshold. Mice deficient for the $\alpha 3$ isoform required a higher threshold charge to trigger SD. Y-axis shows electric charge in micro Coulomb of logarithmically transformed data. (f) In $\alpha 2^{+/KOE4}$ mice, SD speed showed a tendency towards higher values, whereas the speed tended to be lower in $\alpha 3^{+/KOE4}$ animals. Both observations did not reach statistical significance. (g–h) α isoform deficiency had no effect on SD threshold and speed under isoflurane anesthesia. (i) Depression of spontaneous activity following SD was more pronounced in heterozygous knock-out mice of all lines ($\alpha 1$, $\alpha 2$, $\alpha 3$) compared to their wild-type littermates. Differences reached statistical significance ($P < 0.05$) in $\alpha 2$ -het and $\alpha 3$ -het animals ($\alpha 2$: $P = 0.04$, $\alpha 3$: $P = 0.03$). (j) Example of spontaneous activity depression with subsequent recovery. EEG suppression was calculated as RMS amplitude reduction of the bandpass-filtered (1–4 Hz). RMS: root mean square. V_o : extracellularly recorded voltage.

$n = 10$, WT: $29.0 \pm 26.5 \mu\text{C}$, $n = 10$, $P = 0.91$). SD speed trended towards higher values in $\alpha 2$ -deficient mice, although this difference did not reach statistical significance at the 5% level ($\alpha 2^{+/KOE4}$: $5.0 \pm 1.2 \text{ mm/min}$, $n = 9$; WT: $4.2 \pm 1.2 \text{ mm/min}$, $n = 13$; $P = 0.07$) (Figure 5(f)). In contrast to $\alpha 2$ -deficient mice, $\alpha 3^{+/KOE4}$ mice displayed a lower SD speed, although the difference did not reach statistical significance ($\alpha 3^{+/KOE4}$: 3.4 ± 0.8 , $n = 9$; WT: 4.0 ± 0.7 , $n = 8$; $P = 0.07$). Changes in DC and $[\text{K}^+]_o$ during SD did not differ significantly between α isoform deficient mice and WT (Supplementary Figure 3). No significant differences were observed in SD threshold and speed comparing $\alpha 1^{+/KOE15}$, $\alpha 2^{+/KOE4}$, and $\alpha 3^{+/KOE4}$ to WT when using isoflurane anesthesia (Figure 5(g) and (h)).

ECoG depression following SD is pronounced in $\alpha 2$ - and $\alpha 3$ -deficient mice

In electrically active tissue, SD causes spreading depression of spontaneous neuronal activity. To compare ECoG depression between α isoform-deficient mice and WT, we calculated the initial reduction of the root mean square (RMS) amplitude of the bandpass-filtered (1–4 Hz) ECoG following SD. The ECoG depression was more pronounced in $\alpha 2$ isoform-deficient mice ($\alpha 2^{+/KOE4}$: $30.4 \pm 15.5\%$, $n = 10$; WT: $42.2 \pm 10.0\%$, $n = 9$; $P = 0.045$) and $\alpha 3^{+/KOE4}$ mice ($\alpha 3^{+/KOE4}$: $25.0 \pm 7.4\%$, $n = 8$; WT: $34.3 \pm 10.7\%$, $n = 13$; $P = 0.033$) compared to WT. ECoG suppression was not significantly different in $\alpha 1^{+/KOE15}$ compared to WT ($P = 0.4$) (Figure 5(i) and (j)).

The result of a pronounced initial reduction of spontaneous activity with largely normal recovery in $\alpha 2$ -deficient mice is in agreement with data from another $\alpha 2$ knock-out mouse model.⁴² In this study, only $\alpha 2^{+/KOE2}$ mice displayed a difference in the ECoG suppression, whereas the effect was not observed in $\alpha 2^{KOE21}$ mice⁴² indicating different degrees of functional impairment following N- and C-terminal deletions in the knock-out mice. A slowed recovery of the spreading depression as assessed by the spontaneous activity in the ECoG has also been reported in a knock-in mouse model of FHM2,²⁴ whereas evoked potentials recovered in a similar fashion to wild-type animals in the same study and in two FHM1 mouse models.²⁷

Pronounced post SD oligemia in $\alpha 2$ -deficient mice under urethane/ α -chloralose anesthesia

Under physiological conditions, the cerebral hemodynamic response to SD is characterized by a considerable hyperemia followed by a post-SD oligemia in most species, such as humans and rats.⁴³ The rCBF response in mice differs drastically from other studied species⁴¹ (Figure 6(a)). Typical for the vasomotor response in mice is a pronounced fast initial hypoperfusion that is temporally correlated with the DC shift, a short-lasting rCBF recovery, followed by a pronounced oligemic phase that can last up to an hour (Figure 6(b) to (d), Supplementary Figure 4).

rCBF was measured using an LDF probe centered between two ISMEs in the open cranial window of α isoform deficient mice and WT. In $\alpha 2$ -deficient mice, the hypoemic response to SD was significantly more pronounced compared to WT. Both the initial short hypoperfusion ($\alpha 2^{+/KOE4}$: $44.3 \pm 13.9\%$, $n = 10$; $\alpha 2^{+/-}$: $66.8 \pm 21.3\%$, $n = 11$; $p = 0.01$) and the long-lasting hypoemia, as measured 10 min after the short, transient recovery ($\alpha 2^{+/KOE4}$: $53.5 \pm 20.1\%$, $n = 9$; $\alpha 2^{+/-}$: $78.4 \pm 19.1\%$, $n = 11$; $p = 0.009$), decreased by over 30% in $\alpha 2^{+/KOE4}$ mice compared to WT (Figure 6(e) and (f)). No significant differences in the post SD perfusion were apparent in $\alpha 3^{+/KOE14}$ and $\alpha 1^{+/KOE15}$ compared to WT. The pronounced hypoemia in $\alpha 2^{+/KOE4}$ mice suggests a specific role of the $\alpha 2$ isoform in regulation of the diameter of cerebral vasculature.

Discussion

Increased SD susceptibility in brain slices is specific for $\alpha 2$ haploinsufficiency

In this study, we show that the genetic reduction of the three different Na^+/K^+ -ATPase α isoforms expressed in the mammalian brain results in distinct SD phenotypes. Only $\alpha 2^{+/KOE4}$ mice displayed a lower SD threshold in

acute brain slices. In principle, this result is in agreement with studies in FHM2 mouse models and supports evidence that $\alpha 2$ haploinsufficiency results in increased SD susceptibility.^{23–25} However, the threshold effect in $\alpha 2^{+/KOE4}$ mice was only present in acute brain slices when the tissue was exposed to elevated baseline $[\text{K}^+]_o$ for an extended period of time. Under normal conditions, the SD threshold was similar to WT in acute brain slices and in-vivo. These findings present a notable difference in the SD phenotype when compared to data from one of the two published FHM2 knock-in mouse lines ($\alpha 2^{+/W887R}$)^{23,25} and a recent knock-out mouse study,⁴² where an effect on SD threshold was demonstrated under normal $[\text{K}^+]_o$.

Moreover, in normal ACSF, extracellular K^+ clearance during and following intense neuronal stimulation was not significantly compromised in $\alpha 2^{+/KOE4}$ mice. Although this observation is consistent with data from $\alpha 2^{+/G301R}$ mice in a similar protocol,³⁹ it contrasts with the findings in slices of $\alpha 2^{+/W887R}$ mice, that displayed a higher time constant of the $[\text{K}^+]_o$ decay following the stimulation train compared to WT.²⁵

The in-vivo recordings support the findings in acute brain slices from $\alpha 2^{+/KOE4}$ mice. Using two separate experimental paradigms with either urethane/ α -chloralose or isoflurane anesthesia, we found no reduction in the electric charge to trigger SD in $\alpha 2^{+/KOE4}$ mice compared to WT. However, although isoflurane has been employed successfully in SD studies^{44,45} including electrical SD induction,²⁸ the results have to be interpreted with caution, since isoflurane inhibits N-methyl-D-aspartate (NMDA) receptors⁴⁶ and has been reported to suppress SD.^{47–50}

The differences between the mild SD phenotype of $\alpha 2^{+/KOE4}$ mice and published FHM mouse models may be attributable to differences in the genetic modifications of the murine ATP1A2 in knock-out and knock-in mice. Whereas FHM2 mouse models bear missense mutations resulting in the substitution of only a single amino acid,^{23,24} expression of the null allele in $\alpha 2^{+/KOE4}$ mice would lead to an $\alpha 2$ isoform truncated after the first transmembrane domain that would lack approximately 90% of the original protein.¹⁴ In consequence, the protein would be deficient of essential functional elements, such as the nucleotide-binding (N), the phosphorylation (P), and the actuator (A) domain, which is expected to result in full haploinsufficiency.^{51,52}

It seems unlikely that the milder SD phenotype of $\alpha 2^{+/KOE4}$ mice is caused by compensatory overexpression of $\alpha 1$ and/or $\alpha 3$, as semi-quantification of protein and RNA expression has been demonstrated to be at normal levels for $\alpha 1$ and even showed a ~25% reduction in the $\alpha 3$ isoform.²⁶ Moreover, since $\alpha 1$ -deficiency was not associated with increased SD susceptibility and

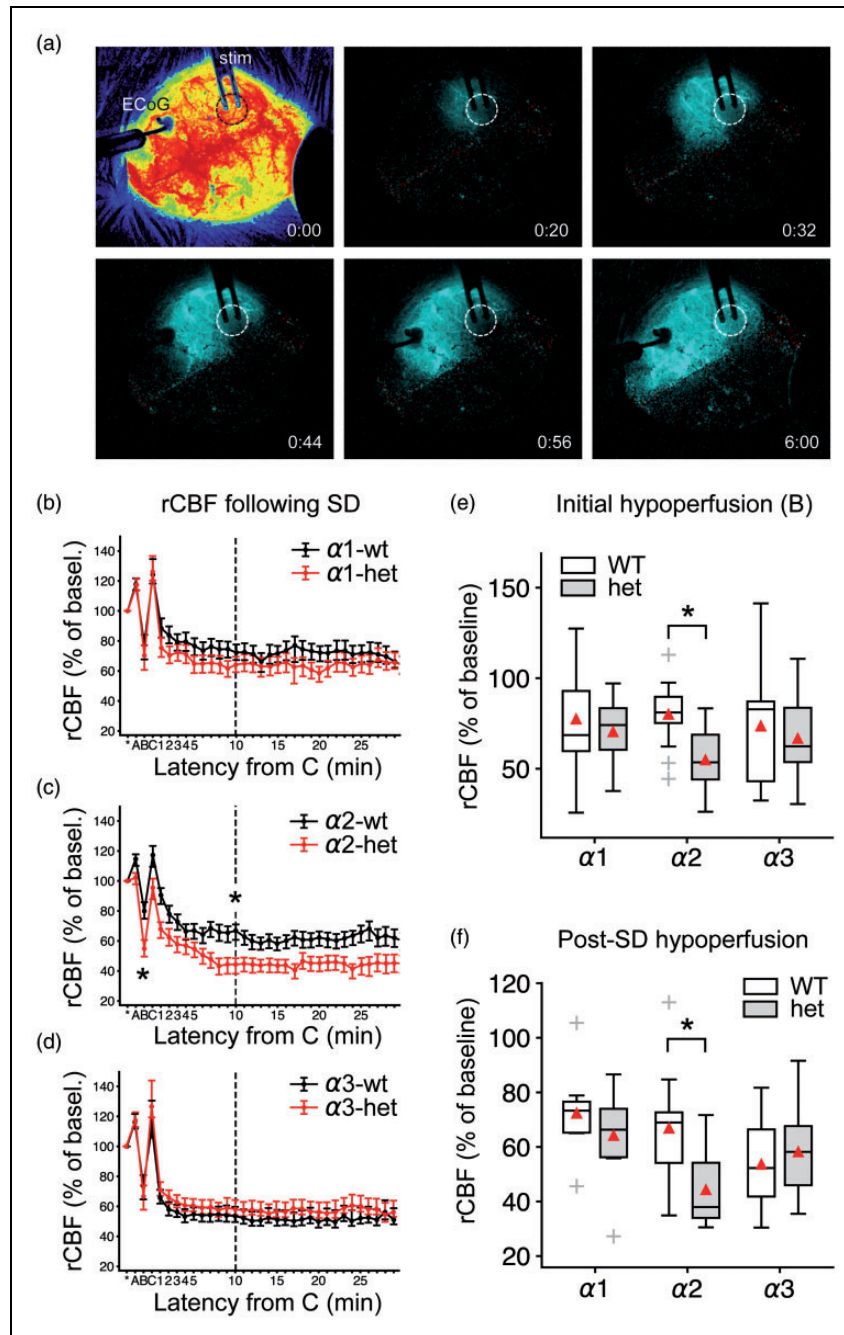


Figure 6. Pronounced hypoperfusion in $\alpha2$ -deficient mice in the wake of SD under urethane/ α -chloralose anesthesia. (a) LASCA imaging in the isoflurane protocol: The first image shows cortical perfusion imaged through the intact mouse skull. Starting from the second image, difference images show the propagating hypoperfusion that characterizes SD in the mouse cortex of the right hemisphere. Regional CBF over time was analyzed and SD speed was calculated. The dashed circle marks the burr hole with the exposed dura mater. Time from SD onset is given in [m:ss] in the lower right. ECoG: electrocorticography, stim: stimulation electrode. (b–d) SD evoked a multiphasic rCBF response in mice denoted A, B, C on the time axis. A: short hyperemia, B: short-lasting hypoemia, C: hyperemia, followed by a long-lasting hypoemia (after C). Data points are given with respect to 5-min baseline rCBF (=100%) prior to SD onset as mean \pm SEM. (e–f) In $\alpha2^{+/KOE4}$ mice, the rCBF following SD showed a pronounced hypoemia in the wake of SD compared to WT during the initial hypoperfusion (marked “B”) and during the long-lasting hypoemia following the short rCBF recovery (marked “C”). By contrast, deficiency of $\alpha1$ and $\alpha3$ did not affect post-SD rCBF.

$\alpha 3^{+/KOE4}$ mice were more resistant against electrical SD induction in-vivo, interpretation of a possible compensatory overexpression would not be straightforward.

Phenotypic variability can also be observed between other mouse models of Na^+/K^+ -ATPase $\alpha 2$ haploinsufficiency. For example, Uekawa et al.⁴² reported higher SD susceptibility in knock-out mice with the N-terminal deletion targeting exon 2 ($\alpha 2^{+/KOE2}$) compared to animals carrying a C-terminal deletion in exon 21 ($\alpha 2^{+/KOE21}$). Heterogeneous results have also been reported for FHM2 knock-in mice. In contrast to $\alpha 2^{+/W887R}$ mice,^{23,25} $\alpha 2^{+/G301R}$ mice displayed a similar SD speed compared to WT²⁴ and did not exhibit a significantly affected $[\text{K}^+]_o$ clearance.³⁹

It seems plausible that differences in experimental approaches contribute to the observed variability of the SD phenotype between different genetically engineered mouse models of $\alpha 2$ deficiency. For example, in this study, we encountered profound SD phenotype differences in the $\alpha 3^{+/KOE4}$ group when using two different experimental approaches in-vivo. The experimental paradigms differed primarily in anesthesia and preparation to gain access to the mouse neocortex for SD induction and recording (open cranial window and ACSF perfusion vs. small burr holes with intact dura mater). Varying anesthetic regimen and SD induction methods have been employed by the other mouse model studies referred to in this article. In the first published FHM-2 mouse model study, Leo et al.²³ used urethane to anesthetize $\alpha 2^{+/W887R}$ knock-in mice and induced SD electrically.²³ By contrast, in the other published FHM-2 mouse model ($\alpha 2^{+/G301R}$), Bottger et al.²⁴ used α -chloralose as the main anesthetic and induced SD by injecting potassium acetate into the neocortical tissue. Yet another approach was used by Uekawa et al.,⁴² who investigated SD susceptibility in two distinct $\alpha 2$ knock-out mice using urethane anesthesia and triggering SD by applying increasing concentrations of KCl solution to the brain surface.

Apart from differences in experimental conditions, the observed phenotypic variability in FHM2 mouse models may reflect the remarkably diverse functional abnormalities described as a consequence of over 80 human disease-linked FHM2 mutations.⁵²

Lack of a single allele of the $\alpha 2$ isoform gene seems to be well compensated in metabolically intact in contrast to stressed tissue

Physiological neuronal activity results in local $[\text{K}^+]_o$ transients of only 0.2–0.4 mM above baseline.^{53,54} During vigorous electrical stimulation, $[\text{K}^+]_o$ locally rises up to the so-called ceiling level of ~ 12 mM.^{54–56} During SD, $[\text{K}^+]_o$ rapidly increases to a level of ~ 50 mM.⁵⁷ In addition to astrocyte-mediated spatial

buffering,^{58–60} the $\alpha 2$ isoform is ideally suited to oppose such acute rises in $[\text{K}^+]_o$ because of its low affinity, which allows the enzyme to rapidly adapt its turnover over a large range of $[\text{K}^+]_o$.^{61,62} In parallel, $\alpha 2$ activity increases in response to the membrane depolarizing effect of rising $[\text{K}^+]_o$,^{63,64} particularly when associated with the $\beta 2$ subunit.³⁹ Further, the maximal catalytic turnover (V_{max}) of the $\alpha 2$ isoform is several fold higher than that of the $\alpha 3$ isoform for example.^{61,65,66}

The $\alpha 2$ isoform is also ideally located to counteract acute rises in extracellular glutamate which typically accompany rises in $[\text{K}^+]_o$. In adult somatosensory cortex of rodents, the $\alpha 2$ enzyme almost completely co-localizes with the astrocytic glutamate transporters GLT-1 (SLC1A2) and GLAST (SLC1A3). Analysis at the ultrastructural level evidenced that this complex preferentially occurs in astrocytic processes around asymmetric glutamatergic synaptic junctions, but not around GABAergic terminals.¹⁶ The $\alpha 2$ isoform is thus assumed to be responsible for the buildup of Na^+ and K^+ gradients necessary for the glutamate uptake in this subcellular microdomain. Impaired $\alpha 2$ function should hence increase the susceptibility to SD based on the notion that SD is a reaction/diffusion mechanism in which neurons release neuroactive substances such as K^+ or glutamate. These are assumed to diffuse to adjacent neurons where they trigger a self-propagating regenerative process.^{67–70} Accordingly, impaired glutamate reuptake was reported in FHM2 knock-in mouse models.^{24,25}

An intriguing interpretation of our results is that the lack of one $\alpha 2$ allele is very well compensated under normal conditions and only becomes apparent in conditions of challenge. Prolonged exposure to elevated $[\text{K}^+]_o$ appears to be such a stressor. This interpretation is, in a broader sense, in agreement with data from a behavioral study of FHM2 knock-in mice ($\alpha 2^{+/G301R}$) that described stress-induced abnormalities when compared with WT.²⁴ Notably, however, elevated baseline $[\text{K}^+]_o$ represents a more extreme and in fact highly pathological stressor, which occurs for example during focal ischemia or after brain hemorrhage. Whereas hemolysis is the source of K^+ in brain hemorrhage,⁷¹ ischemia causes activation of Ca^{2+} -activated K^+ channels, resulting in a rise of baseline $[\text{K}^+]_o$, long before the ATP shortage slows the Na^+/K^+ -ATPases and SD occurs associated with further rapid rise of $[\text{K}^+]_o$.^{72,73}

Because expression of the $\alpha 2$ isoform is reduced by about $\sim 50\%$ in $\alpha 2^{+/KOE4}$ mice,²⁶ it is conceivable that the reduced gene dosage is unmasked only in conditions where transport capacity is exhausted and adaptation would require upregulation. Regulation of the intrinsic Na^+/K^+ -ATPase activity depends on substrate

concentration (K^+ , Na^+ , ATP), interaction with FXYD proteins and covalent modification, such as glutathionylation and phosphorylation.^{36,74} Further activity increase requires the insertion of additional Na^+/K^+ -ATPase enzymes into the plasma membrane through mobilization from endosomal pools,^{74,75} which might consequently unmask a reduced protein expression.

An additional mechanism could potentially aggravate $\alpha 2$ isoform deficiency under conditions of high $[K^+]_o$ load and promote decompensation of its homeostatic function: Previous studies have demonstrated a decrease of the ouabain-suppressible $\alpha 2/\alpha 3$ portion of the total Na^+/K^+ -ATPase activity in response to elevated baseline $[K^+]_o$. It has been suggested that this reduction did not result from loss of high-energy phosphate levels or modifications in protein or mRNA expression but from modifications of specific active sites, trapping the enzyme in an inactive phosphorylated state.⁷⁶

Pronounced post-SD oligemia in $\alpha 2$ -deficient mice

Mice deficient of the $\alpha 2$ isoform showed pronounced post-SD hypoemic responses. This could result from abnormal Ca^{2+} handling leading to enhanced vasoconstriction in the wake of SD. A multitude of studies have pointed to a distinct role of the $\alpha 2$ isoform in controlling local Ca^{2+} concentration and thereby modulating the release from intracellular Ca^{2+} stores.⁷⁷ Functional coupling of the $\alpha 2$ isoform with the Na^+/Ca^{2+} -exchanger (NCX)⁷⁸ was proposed as the mechanism by which the local Ca^{2+} concentration increases and in consequence the concentration in the endoplasmic/sarcoplasmic reticulum.⁷⁹ In the brain, the $\alpha 2$ isoform is highly expressed in glial and vascular smooth muscle cells (VSMCs) and the observed vasoconstrictive effect could be mediated by augmented intracellular Ca^{2+} transients in either cell type. In VSMCs and astrocytes, ouabain has been found to induce intracellular Ca^{2+} increases.^{12,15} Augmented Ca^{2+} transients in astrocytic endfeet were reported to cause constriction in arterioles.⁸⁰ The pronounced hypoemic rCBF response in $\alpha 2^{+/KOE4}$ mice is in agreement with data from $\alpha 2^{+/G301R}$ mice that have been described to exhibit enhanced contractility of cerebral arteries.⁸¹ This study identified higher Ca^{2+} sensitivity as opposed to increased Ca^{2+} release as the cause of enhanced contractility. The effect was reversible by cSrc inhibition. In addition, the resting blood flow in the middle cerebral artery was reduced in $\alpha 2^{+/G301R}$ mice.

Higher SD resistance of $\alpha 3$ -deficient mice in-vivo

Despite significant Na^+/K^+ -ATPase reduction in whole brain homogenates, $\alpha 3^{+/KOE4}$ mice were more resistant

against electrically induced SD in-vivo under urethane/ α -chloralose anesthesia compared to WT and displayed a lower SD speed. In a behavioral study, $\alpha 3^{+/KOE4}$ mice were shown to have a $\sim 40\%$ lower hippocampal NMDA receptor NR1 isoform expression compared to WT and more pronounced learning deficits compared to $\alpha 2$ -deficient mice.²⁶ One possible explanation of the decreased NMDA receptor expression is that chronic overexcitability during development may result in compensatory NMDA downregulation to reduce excitotoxic damage to neurons. Reduced glutamate receptor availability could explain the diminished efficiency of electrical SD induction since the induction process is likely to depend on glutamate release.⁸²

Conclusion

In summary, the data demonstrate distinct SD phenotypes as a consequence of genetic disruption or pharmacological inhibition of the three Na^+/K^+ -ATPase α isoforms expressed in the brain. Both, the astrocytic and neuronal isoform differentially affect the SD phenotype in heterozygous knock-out mice, whereas lack of one allele of $\alpha 1$, the ubiquitous isoform, had no significant effect on SD-associated features.

The dependence on additional external factors to reveal the SD phenotype in $\alpha 2^{+/KOE4}$ mice presents a mechanism that may model the episodic nature of migraine aura, where attacks depend on a combination of genetically determined susceptibility and challenging environmental conditions.⁸² In addition, the presented features of the different Na^+/K^+ -ATPase α isoforms are important for conditions during which the SD continuum is now increasingly recorded while the patient is on the neurocritical care unit, such as traumatic brain injury, intracerebral spontaneous hematoma, aneurysmal subarachnoid hemorrhage, malignant hemispheric stroke or cardiac arrest.^{1,83} Better understanding of the different isoforms could inform the development of novel therapeutic strategies in all these conditions.

Acknowledgements

We would like to thank Prof. Jerry B. Lingrel for generously providing heterozygous knock-out mice of ATP1A1, ATP1A2, and ATP1A3.

Author's contributions

Clemens Reiffurth: designed and performed experiments in-vivo, in acute brain slices and in-vitro, analyzed data, drafted and finalized the manuscript and approved the manuscript before submission. Mesbah Alam: designed and performed experiments in-vivo and in acute brain slices, analyzed data and approved the manuscript before submission. Mahdi Zahedi: designed and performed experiments in acute brain

slices, analyzed data and approved the manuscript before submission. Sebastian Major: designed experiments, analyzed data and approved the manuscript before submission. Jens Dreier: planned the study, designed experiments, analyzed data, drafted and finalized the manuscript and approved the manuscript before submission.

Funding

The author(s) disclosed receipt of the following financial support for the research, authorship, and/or publication of this article: This work was supported by Deutsche Forschungsgemeinschaft (DFG DR 323/5-1 and DFG DR 323/10-1), the Bundesministerium für Bildung und Forschung (Center for Stroke Research Berlin, 01 EO 0801) and FP7 no 602150 CENTER-TBI to Dr. Dreier.

Declaration of conflicting interests

The author(s) declared no potential conflicts of interest with respect to the research, authorship, and/or publication of this article.

ORCID iD

Jens P Dreier  <http://orcid.org/0000-0001-7459-2828>

Supplementary material

Supplementary material for this paper can be found at the journal website: <http://journals.sagepub.com/home/jcb>

References

- Dreier JP and Reiffurth C. The stroke-migraine depolarization continuum. *Neuron* 2015; 86: 902–922.
- Hartings JA, Shuttleworth CW, Kirov SA, et al. The continuum of spreading depolarizations in acute cortical lesion development: examining Leao's legacy. *J Cereb Blood Flow Metab* 2017; 37: 1571–1594.
- Engl E and Attwell D. Non-signalling energy use in the brain. *J Physiol* 2015; 593: 3417–3429.
- Astrup J, Sorensen PM and Sorensen HR. Oxygen and glucose consumption related to Na⁺-K⁺ transport in canine brain. *Stroke* 1981; 12: 726–730.
- Balestrino M, Young J and Aitken P. Block of (Na⁺,K⁺)ATPase with ouabain induces spreading depression-like depolarization in hippocampal slices. *Brain Res* 1999; 838: 37–44.
- Balestrino M. Pathophysiology of anoxic depolarization: new findings and a working hypothesis. *J Neurosci Methods* 1995; 59: 99–103.
- Kager H, Wadman WJ and Somjen GG. Conditions for the triggering of spreading depression studied with computer simulations. *J Neurophysiol* 2002; 88: 2700–2712.
- McGrail KM, Phillips JM and Sweadner KJ. Immunofluorescent localization of three Na,K-ATPase isozymes in the rat central nervous system: both neurons and glia can express more than one Na,K-ATPase. *J Neurosci* 1991; 11: 381–391.
- Orlowski J and Lingrel JB. Tissue-specific and developmental regulation of rat Na,K-ATPase catalytic alpha isoform and beta subunit mRNAs. *J Biol Chem* 1988; 263: 10436–10442.
- O'Brien WJ, Lingrel JB and Wallick ET. Ouabain binding kinetics of the rat alpha two and alpha three isoforms of the sodium-potassium adenosine triphosphate. *Arch Biochem Biophys* 1994; 310: 32–39.
- Moseley AE, Lieske SP, Wetzel RK, et al. The Na,K-ATPase alpha 2 isoform is expressed in neurons, and its absence disrupts neuronal activity in newborn mice. *J Biol Chem* 2003; 278: 5317–5324.
- Juhaszova M and Blaustein MP. Na⁺ pump low and high ouabain affinity alpha subunit isoforms are differently distributed in cells. *Proc Natl Acad Sci U S A* 1997; 94: 1800–1805.
- Hartford AK, Messer ML, Moseley AE, et al. Na,K-ATPase alpha 2 inhibition alters calcium responses in optic nerve astrocytes. *Glia* 2004; 45: 229–237.
- James PF, Grupp IL, Grupp G, et al. Identification of a specific role for the Na,K-ATPase alpha 2 isoform as a regulator of calcium in the heart. *Mol Cell* 1999; 3: 555–563.
- Song H, Lee MY, Kinsey SP, et al. An N-terminal sequence targets and tethers Na⁺ pump alpha2 subunits to specialized plasma membrane microdomains. *J Biol Chem* 2006; 281: 12929–12940.
- Similar perisynaptic glial localization for the Na⁺,K⁺-ATPase alpha 2 subunit and the glutamate transporters GLAST and GLT-1 in the rat somatosensory cortex. *Cereb Cortex* 2002; 12: 515–525.
- Rose EM, Koo JC, Antflick JE, et al. Glutamate transporter coupling to Na,K-ATPase. *J Neurosci* 2009; 29: 8143–8155.
- De Fusco M, Marconi R, Silvestri L, et al. Haploinsufficiency of ATP1A2 encoding the Na⁺/K⁺ pump alpha2 subunit associated with familial hemiplegic migraine type 2. *Nat Genet* 2003; 33: 192–196.
- de Carvalho Aguiar P, Sweadner KJ, Penniston JT, et al. Mutations in the Na⁺/K⁺-ATPase alpha3 gene ATP1A3 are associated with rapid-onset dystonia parkinsonism. *Neuron* 2004; 43: 169–175.
- Heinzen EL, Swoboda KJ, Hitomi Y, et al. De novo mutations in ATP1A3 cause alternating hemiplegia of childhood. *Nat Genet* 2012; 44: 1030–1034.
- Rosewich H, Thiele H, Ohlenbusch A, et al. Heterozygous de-novo mutations in ATP1A3 in patients with alternating hemiplegia of childhood: a whole-exome sequencing gene-identification study. *Lancet Neurol* 2012; 11: 764–773.
- Demos MK, van Karnebeek CD, Ross CJ, et al. A novel recurrent mutation in ATP1A3 causes CAPOS syndrome. *Orphanet J Rare Dis* 2014; 9: 15.
- Leo L, Gherardini L, Barone V, et al. Increased susceptibility to cortical spreading depression in the mouse model of familial hemiplegic migraine type 2. *PLoS Genet* 2011; 7: e1002129.
- Bottger P, Glerup S, Gesslein B, et al. Glutamate-system defects behind psychiatric manifestations in a familial hemiplegic migraine type 2 disease-mutation mouse model. *Sci Rep* 2016; 6: 22047.

25. Capuani C, Melone M, Tottene A, et al. Defective glutamate and K⁺ clearance by cortical astrocytes in familial hemiplegic migraine type 2. *EMBO Mol Med* 2016; 8: 967–986.
26. Moseley AE, Williams MT, Schaefer TL, et al. Deficiency in Na,K-ATPase alpha isoform genes alters spatial learning, motor activity, and anxiety in mice. *J Neurosci* 2007; 27: 616–626.
27. Eikermann-Haerter K, Dilekoz E, Kudo C, et al. Genetic and hormonal factors modulate spreading depression and transient hemiparesis in mouse models of familial hemiplegic migraine type 1. *J Clin Invest* 2009; 119: 99–109.
28. Brennan KC, Romero Reyes M, Lopez Valdes HE, et al. Reduced threshold for cortical spreading depression in female mice. *Ann Neurol* 2007; 61: 603–606.
29. Holmdahl R and Malissen B. The need for littermate controls. *Eur J Immunol* 2012; 42: 45–47.
30. Taylor CP, Weber ML, Gaughan CL, et al. Oxygen/glucose deprivation in hippocampal slices: altered intraneuronal elemental composition predicts structural and functional damage. *J Neurosci* 1999; 19: 619–629.
31. Kirov SA, Sorra KE and Harris KM. Slices have more synapses than perfusion-fixed hippocampus from both young and mature rats. *J Neurosci* 1999; 19: 2876–2886.
32. Schurr A, Reid KH, Tseng MT, et al. The stability of the hippocampal slice preparation: an electrophysiological and ultrastructural analysis. *Brain Res* 1984; 297: 357–362.
33. van den Maagdenberg AM, Pietrobon D, Pizzorusso T, et al. A Cacna1a knockin migraine mouse model with increased susceptibility to cortical spreading depression. *Neuron* 2004; 41: 701–710.
34. Oliphant TE. Python for Scientific Computing. *Computing in Science & Engineering* 2007; 9: 10–20.
35. Hunter JD. Matplotlib: a 2D graphics environment. *Comput Sci Eng* 2007; 9: 90–95.
36. Blanco G and Mercer RW. Isozymes of the Na-K-ATPase: heterogeneity in structure, diversity in function. *Am J Physiol* 1998; 275: F633–F650.
37. Heinemann U and Lux HD. Undershoots following stimulus-induced rises of extracellular potassium concentration in cerebral cortex of cat. *Brain Res* 1975; 93: 63–76.
38. Wallraff A, Kohling R, Heinemann U, et al. The impact of astrocytic gap junctional coupling on potassium buffering in the hippocampus. *J Neurosci* 2006; 26: 5438–5447.
39. Stoica A, Larsen BR, Assentoft M, et al. The alpha2beta2 isoform combination dominates the astrocytic Na(+)/K(+)-ATPase activity and is rendered nonfunctional by the alpha2.G301R familial hemiplegic migraine type 2-associated mutation. *Glia* 2017; 65: 1777–1793.
40. Tottene A, Conti R, Fabbro A, et al. Enhanced excitatory transmission at cortical synapses as the basis for facilitated spreading depression in Ca(v)2.1 knockin migraine mice. *Neuron* 2009; 61: 762–773.
41. Ayata C, Shin HK, Salomone S, et al. Pronounced hypoperfusion during spreading depression in mouse cortex. *J Cereb Blood Flow Metab* 2004; 24: 1172–1182.
42. Unekawa M, Ikeda K, Tomita Y, et al. Enhanced susceptibility to cortical spreading depression in two types of Na(+),K(+)-ATPase alpha2 subunit-deficient mice as a model of familial hemiplegic migraine 2. *Cephalalgia* 2018; 38: 1515–1524.
43. Ayata C and Lauritzen M. Spreading depression, spreading depolarizations, and the cerebral vasculature. *Physiol Rev* 2015; 95: 953–993.
44. Cain SM, Bohnet B, LeDue J, et al. In vivo imaging reveals that pregabalin inhibits cortical spreading depression and propagation to subcortical brain structures. *Proc Natl Acad Sci U S A* 2017; 114: 2401–2406.
45. Eikermann-Haerter K, Arbel-Ornath M, Yalcin N, et al. Abnormal synaptic Ca(2+) homeostasis and morphology in cortical neurons of familial hemiplegic migraine type 1 mutant mice. *Ann Neurol* 2015; 78: 193–210.
46. Dickinson R, Peterson BK, Banks P, et al. Competitive inhibition at the glycine site of the N-methyl-D-aspartate receptor by the anesthetics xenon and isoflurane: evidence from molecular modeling and electrophysiology. *Anesthesiology* 2007; 107: 756–767.
47. Saito R, Graf R, Hubel K, et al. Halothane, but not alpha-chloralose, blocks potassium-evoked cortical spreading depression in cats. *Brain Res* 1995; 699: 109–115.
48. Guedes RC and Barreto JM. Effect of anesthesia on the propagation of cortical spreading depression in rats. *Braz J Med Biol Res* 1992; 25: 393–397.
49. Kudo C, Nozari A, Moskowitz MA, et al. The impact of anesthetics and hyperoxia on cortical spreading depression. *Exp Neurol* 2008; 212: 201–206.
50. Takagaki M, Feuerstein D, Kumagai T, et al. Isoflurane suppresses cortical spreading depolarizations compared to propofol – implications for sedation of neurocritical care patients. *Exp Neurol* 2014; 252: 12–17.
51. Morth JP, Pedersen BP, Toustrup-Jensen MS, et al. Crystal structure of the sodium-potassium pump. *Nature* 2007; 450: 1043–1049.
52. Friedrich T, Tavraz NN and Junghans C. ATP1A2 mutations in migraine: seeing through the facets of an ion pump onto the neurobiology of disease. *Front Physiol* 2016; 7: 239.
53. Sykova E, Rothenberg S and Krekule I. Changes of extracellular potassium concentration during spontaneous activity in the mesencephalic reticular formation of the rat. *Brain Res* 1974; 79: 333–337.
54. Heinemann U and Lux HD. Ceiling of stimulus induced rises in extracellular potassium concentration in the cerebral cortex of cat. *Brain Res* 1977; 120: 231–249.
55. Prince DA, Lux HD and Neher E. Measurement of extracellular potassium activity in cat cortex. *Brain Res* 1973; 50: 489–495.
56. Futamachi KJ, Mutani R and Prince DA. Potassium activity in rabbit cortex. *Brain Res* 1974; 75: 5–25.
57. Vyskocil F, Kritz N and Bures J. Potassium-selective microelectrodes used for measuring the extracellular brain potassium during spreading depression and anoxic depolarization in rats. *Brain Res* 1972; 39: 255–259.

58. Karwoski CJ, Lu HK and Newman EA. Spatial buffering of light-evoked potassium increases by retinal Muller (glial) cells. *Science* 1989; 244: 578–580.
59. Walz W. Role of astrocytes in the clearance of excess extracellular potassium. *Neurochem Int* 2000; 36: 291–300.
60. Kofuji P and Newman EA. Potassium buffering in the central nervous system. *Neuroscience* 2004; 129: 1045–1056.
61. Walz W and Hertz L. Ouabain-sensitive and ouabain-resistant net uptake of potassium into astrocytes and neurons in primary cultures. *J Neurochem* 1982; 39: 70–77.
62. Grisar T, Franck G and Schoffeniels E. Glial control of neuronal excitability in mammals: II. Enzymatic evidence: two molecular forms of the (Na(+),K(+))-ATPase in brain. *Neurochem Int* 1980; 2: 311–320.
63. Crambert G, Hasler U, Beggah AT, et al. Transport and pharmacological properties of nine different human Na, K-ATPase isozymes. *J Biol Chem* 2000; 275: 1976–1986.
64. Horisberger JD and Kharoubi-Hess S. Functional differences between alpha subunit isoforms of the rat Na,K-ATPase expressed in *Xenopus* oocytes. *J Physiol* 2002; 539: 669–680.
65. Kimelberg HK, Biddelcome S, Narumi S, et al. ATPase and carbonic anhydrase activities of bulk-isolated neuron, glia and synaptosome fractions from rat brain. *Brain Res* 1978; 141: 305–323.
66. Hajek I, Subbarao KV and Hertz L. Acute and chronic effects of potassium and noradrenaline on Na⁺, K⁺-ATPase activity in cultured mouse neurons and astrocytes. *Neurochem Int* 1996; 28: 335–342.
67. Dreier JP, Lemale CL, Kola V, et al. Spreading depolarization is not an epiphenomenon but the principal mechanism of the cytotoxic edema in various gray matter structures of the brain during stroke. *Neuropharmacology* 2018; 134: 189–207.
68. Zhou N, Rungta RL, Malik A, et al. Regenerative glutamate release by presynaptic NMDA receptors contributes to spreading depression. *J Cereb Blood Flow Metab* 2013; 33: 1582–1594.
69. Zandt BJ, ten Haken B and van Putten MJ. Diffusing substances during spreading depolarization: analytical expressions for propagation speed, triggering, and concentration time courses. *J Neurosci* 2013; 33: 5915–5923.
70. Moskowitz MA, Bolay H and Dalkara T. Deciphering migraine mechanisms: clues from familial hemiplegic migraine genotypes. *Ann Neurol* 2004; 55: 276–280.
71. Ohta O, Siguma M, Yamamoto M, Shimizu K and Toda N. *Cerebral vasospasm following ruptured intracranial aneurysms, especially some contributions of potassium ion released from subarachnoid hematoma to delayed cerebral vasospasm*. New York: Raven Press, 1998.
72. Erdemli G, Xu YZ and Krnjevic K. Potassium conductance causing hyperpolarization of CA1 hippocampal neurons during hypoxia. *J Neurophysiol* 1998; 80: 2378–2390.
73. Revah O, Lasser-Katz E, Fleidervish IA, et al. The earliest neuronal responses to hypoxia in the neocortical circuit are glutamate-dependent. *Neurobiol Dis* 2016; 95: 158–167.
74. Pirkmajer S and Chibalin AV. Na,K-ATPase regulation in skeletal muscle. *Am J Physiol Endocrinol Metab* 2016; 311: E1–E31.
75. Ewart HS and Klip A. Hormonal regulation of the Na(+)-K(+)-ATPase: mechanisms underlying rapid and sustained changes in pump activity. *Am J Physiol* 1995; 269: C295–311.
76. Mishra OP and Delivoria-Papadopoulos M. Cellular mechanisms of hypoxic injury in the developing brain. *Brain Res Bull* 1999; 48: 233–238.
77. Golovina VA, Song H, James PF, et al. Na⁺ pump alpha 2-subunit expression modulates Ca²⁺ signaling. *Am J Physiol Cell Physiol* 2003; 284: C475–486.
78. DiPolo R and Beauge L. Sodium/calcium exchanger: influence of metabolic regulation on ion carrier interactions. *Physiol Rev* 2006; 86: 155–203.
79. Moore ED, Etter EF, Philipson KD, et al. Coupling of the Na⁺/Ca²⁺ exchanger, Na⁺/K⁺ pump and sarcoplasmic reticulum in smooth muscle. *Nature* 1993; 365: 657–660.
80. Girouard H, Bonev AD, Hannah RM, et al. Astrocytic endfoot Ca²⁺ and BK channels determine both arteriolar dilation and constriction. *Proc Natl Acad Sci U S A* 2010; 107: 3811–3816.
81. Staehr C, Hangaard L, Bouzinova EV, et al. Smooth muscle Ca(2+) sensitization causes hypercontractility of middle cerebral arteries in mice bearing the familial hemiplegic migraine type 2 associated mutation. *J Cereb Blood Flow Metab*. Epub ahead of print 7 March 2018. DOI: 10.1177/0271678X18761712.
82. Pietrobon D and Moskowitz MA. Pathophysiology of migraine. *Annu Rev Physiol* 2013; 75: 365–391.
83. Dreier JP, Major S, Foreman B, et al. Terminal spreading depolarization and electric silence in death of human cortex. *Ann Neurol* 2018; 83: 295–310.